Controlled information transfer in continuous-time chiral quantum walks

New Journal of Physics
The open access journal at the forefront of physics

Deutsche Physikalische Gesellschaft DPG IOP Institute of Physics

Controlled information transfer in continuous-time chiral quantum walks

New Journal of Physics
The open access journal at the forefront of physics

Deutsche Physikalische Gesellschaft DPG
IOP Institute of Physics

Published in partnership with: Deutsche Physikalische Gesellschaft and the Institute of Physics

OPEN ACCESS

RECEIVED
10 April 2021

REVISED
28 June 2021

ACCEPTED FOR PUBLICATION
16 July 2021

PUBLISHED
4 August 2021

PAPER

Controlled information transfer in continuous-time chiral quantum walks

A Khalique[1,2,*], A Sett[3], J B Wang[3] and J Twamley[4,5]

[1] School of Natural Sciences, National University of Sciences and Technology, Islamabad, Pakistan
[2] National Centre for Physics (NCP), Shahdra Valley Road, Islamabad 44000, Pakistan
[3] Department of Physics, The University of Western Australia, Perth, WA 6009, Australia
[4] Quantum Machines Unit, Okinawa Institute of Science and Technology Graduate University, Okinawa 904-0495, Japan
[5] Centre for Engineered Quantum Systems, Department of Physics and Astronomy, Macquarie University, Sydney, New South Wales 2109, Australia
[*] Author to whom any correspondence should be addressed.

E-mail: aeysha.khalique@sns.nust.edu.pk

Keywords: quantum walk, quantum transport, directed quantum transport, non-Markovian quantum process

Abstract

In this paper we investigate properties of continuous time chiral quantum walks, which possess complex valued edge weights in the underlying graph structure, together with an initial Gaussian wavefunction spread over a number of vertices. We demonstrate that, for certain graph topology and phase matching conditions, we are able to direct the flow of probability amplitudes in a specific direction inside the graph network. We design a quantum walk graph analogue of an optical circulator which is a combination of a cycle and semi-infinite chain graphs. Excitations input into the circulator from a semi-infinite chain are routed in a directionally biased fashion to output to a different semi-infinite chain. We examine in detail a two port circulator graph which spatially separates excitations flowing back in forth between the two semi-finite chains to directionally occupy the top or bottom half of the cycle portion of the circulator. This setup can be used, for example, to detect non-Markovian processes, which leads to information and energy back-flow from the bath back into the system.

1. Introduction

Quantum walks provide a quantum analogue of classical random walks [1]. Different from a classical walker, a quantum walker can be in a superposition state and can co-exist at many vertices. The interference of these superposition states result in extraordinary probability distributions of the walker at different positions over time [2, 3]. In continuous-time quantum walks (CTQW), the walker traverses various vertices following a Hamiltonian evolution [4–7]. The CTQW model of quantum computing [8] is shown to be universal [9], which makes CTQWs a general platform for developing quantum software and applications.

The basic quantum postulates require that in CTQW, the time evolution must be unitary. To achieve a directional bias for the walker's dynamics while keeping the time evolution unitary has proved challenging in the literature. Previously, directionality has been incorporated in quantum stochastic walks [10–13] through non-unitary evolution of open quantum systems described by the Lindblad equation [14]. Other methods to achieve biased transport include using a time-dependent Hamiltonian [15] and Hamiltonian with PT-symmetry [16–18] or a unitary-dilation approach [19]. Recently, zero transfer has been proposed in CTQW by weighted edges [20].

In this work, we engineer a spatially biased CTQW but we do so in a manner which neither uses time dependent Hamiltonians nor non-unitary evolution. Instead we will draw upon our previous work [21], used to achieve directed transfer in path and cycle configurations of wave guides with varying propagation

constants and show how a similarly constructed Hamiltonian achieves directed transfer in chiral quantum walks (CQW) on path and cycle graphs. We show that with a certain arrangement of edge weights directed transfer can be achieved in path and cycle graphs and a combination path and cycle graphs (which we denote as the *circulator graph* (CG)), using an initial state which is a Gaussian wave packet spread over a number of sites [22, 23]. We investigate the behaviour of directed transfer in these graphs as a function of the initial width of the Gaussian wave packet. We study the potential use of the combination CG to flag the direction of energy transport. Similar to a normal optical circulator we find that this CG can be used to direct different inputs to different outputs. We show that when operating with an initial Gaussian wave-packet, this CG can be used to detect non-Markovianity or channel noise, which leads to information back-flow. This is achieved by changing the weights of certain edges.

The paper is organized as follows: in section 2, we give a short background on graph theory and CTQWs. In section 3 we explain our approach for directed transfer for path and cycle graphs and for a combination of the two—the CG. We describe how a CTQW on the CG can be used as a way to detect non-Markovianity in a coupling to a bath, indicating when information/excitation flows back into the system from the bath in section 4. We explore the dependence of the initial Gaussian wave-packet width on directed transfer and relate it to uncertainty principle in section 5. Finally we conclude in section 6.

2. Background

A graph G comprises a set of vertices V and a set of edges E, where each edge contains a pair of vertices (a, b) such that $a, b \in V$. In directed graphs the pair (a, b) represents an edge from a to b, the vertices are then said to be adjacent. We can construct an adjacency matrix A such $A_{ij} = w_{ij}$ [24], where w_{ij} is the weight of an edge, which can be real or complex. $A_{ij} = 0$ if an edge does not exist between two vertices.

The vertices can be connected in a variety of ways. If each vertex is adjacent to the previous one, then graph G is called a path. A *cycle* is a path where the first and last vertex in the sequence that describes the path is the same. The cycle graph with n vertices is denoted by C_n [25]. In this work we are in particularly interested in a combination of path and cycle graphs.

Quantum walks may be discrete [1] or continuous [8]. Continuous time quantum walk (CTQW) is the quantum analogue of the continuous time classical random walk [26]. For a graph G with n vertices, the state of the walker at any time t is $|\psi(t\rangle)$ and is given in the set of n orthonormal basis $\{|1\rangle, |2\rangle, \ldots, |n\rangle\}$, where each $|i\rangle$ is the state occupying the ith vertex. The unitary time evolution of the walker initially in state $|\psi(0)\rangle$,

$$\begin{aligned} |\psi(t\rangle) &= U|\psi(0)\rangle \\ &= \mathrm{e}^{-\mathrm{i}\widehat{H}t/\hbar}|\psi(0)\rangle, \end{aligned} \tag{1}$$

is governed by the Hamiltonian H. The Hamiltonian H is Hermitian and is equal to the adjacency matrix A [26]. A weighted adjacency matrix with elements

$$\begin{aligned} A_{ij} &= h_{ij} \quad \text{for } (i,j) \in E(G) \\ &= 0 \quad \text{otherwise} \end{aligned} \tag{2}$$

has $h_{ij} = h_{ji}$, for A and hence H is Hermitian. An interesting phenomena is the CQW, where the edge weights are complex and involve complex phases in the adjacency matrix

$$\begin{aligned} A_{ij}^{'} &= \mathrm{e}^{\mathrm{i}\alpha_{ij}} h_{ij} \quad \text{for } (i,j) \in E(G) \\ &= 0 \quad \text{otherwise}, \end{aligned} \tag{3}$$

where $\alpha_{ij} = -\alpha_{ji}$ and $h_{ij} = h_{ji}$ for hermiticity. More specifically, each edge in the original graph becomes two directed edges in opposite directions with complex edge weights which are complex conjugates of each other.

The time evolution of the walker depends on both the adjacency matrix A and the initial state $|\psi(0)\rangle$ of the walker. The initial state of the walker plays a vital role in the directed transfer described below.

3. Directed transfer

Directed transfer arranges the walker to move in a certain preferred directions while suppressing movement in other, unwanted directions. Controlled time-asymmetric transport in a palindromic quantum circuits

has been demonstrated experimentally with high fidelity using local gates where the walker is initialized at a single vertex [27]. This work, although demonstrating enhanced chiral transfer probabilities, does not lead to complete control of the direction of propagation due primarily to the single-vertex localisation of their initial state. Initial states which are not localised on a single vertex have been used in various quantum walk algorithms. These include spatial search algorithm with initial state as superposition of all the vertices [9], and the quantum NAND tree algorithm [8], where the initial state is taken as a Gaussian wave-packet over a subset of vertices. It has been reported that the Gaussian wave-packet is often a promising initial state for modelling physical phenomena [28].

It is often assumed that the unitarity of the time evolution of a CTQW and CQW makes the standard quantum walk model incapable of demonstrating directed transfer. Two approaches have been used so far to achieve directed transfer in quantum walks. First, non-unitary evolution, which can be achieved by coupling the walk to open quantum systems via evolution described by Lindblad equation [14], can lead to directionality [10] in a CTQW. Second, time-dependent Hamiltonian operators [21] have been proposed for directed transfer.

In this work we describe how to achieve directed transfer without resorting to non-unitary dynamics or a time-dependent Hamiltonian. A central ingredient in our protocol is the choice of the initial state to be a Gaussian wave-packet, distributed over a number of adjacent vertices. We choose this type of initial state so that the initial state has a well defined position and momentum and evolves in a manner which has low dispersion and whose direction of propagation on the graph can be highly directed though the introduction of complex edge weights. We find that we can control the propagation directions by manipulating the initial Gaussian state and by engineering destructive interference along unwanted paths in the graphs. We achieve the extreme case of transport enhancement and suppression in path, cycle and circulant graphs, thus allowing the transfer of information preferentially along certain directions.

In this paper we will define our unnormalised initial state to be a Gaussian wave on some subset of vertices of the graph, $V_{\text{in}} \subseteq V(G)$, as

$$\sum_{j\in V_{\text{in}}} \exp\left(\frac{-d(v_{\text{mid}},j)^2}{2\sigma^2}\right)|j\rangle, \tag{4}$$

where the wave is centred at v_{mid} and has width, σ. $d(v_{\text{mid}},j)$ is some distance measure between v_{mid} and vertex j. For the graphs that we consider, the path graph and cycle graph, V_{in} will always consist of adjacent vertices on a path hence we will define $d(v_{\text{mid}},j)$ and V_{in} as

$$d(v_{\text{mid}},j) = |v_{\text{mid}} - j|, \tag{5}$$

$$V_{\text{in}} = V(G), \tag{6}$$

where we use a lexicographical ordering of vertex labels.

We consider the dynamics of a CTQW over a graph containing N vertices, where we can depict the vertices as being spatially distributed, and coupled via a nearest-neighbour Hamiltonian [21], given by

$$H = H_\sigma + H_\omega, \tag{7}$$

where

$$H_\sigma = \sum_{j=1}^{N_0}\left(J_{j,j+1}\sigma_j\sigma_{j+1}^\dagger + \text{h.c.}\right), \tag{8}$$

and

$$H_\omega = \sum_{j=1}^{N}\omega_j\sigma_j\sigma_j^\dagger. \tag{9}$$

$J_{j,j+1}$ is the interaction energy between site j and site $j+1$, ω_j is self-energy of site j and $\sigma_j^\dagger$ and σ_j are the creation and annihilation operators of site j respectively [21]. For path configurations $N_0 = N-1$. For cycle configurations $N_0 = N$ and $N_0 + 1 = 1$. In general, the term $J_{j,j+1}\sigma_j^\dagger\sigma_{j+1}$ can be interpreted as a weighted directed edge from vertex j to $j+1$. The same holds for the Hermitian conjugate term (h.c.), $J_{j+1,j}\sigma_{j+1}^\dagger\sigma_j$, which is interpreted as a directed edge from vertex $j+1$ to j. The state vector, $|\psi(t)\rangle$, satisfies Schrödinger's equation

$$|\psi(t)\rangle = U(t)|\psi(0)\rangle, \tag{10}$$

where $U(t) = \mathrm{e}^{-\mathrm{i}Ht/\hbar}$ and $|\psi(0)\rangle$ is the initial wave vector.

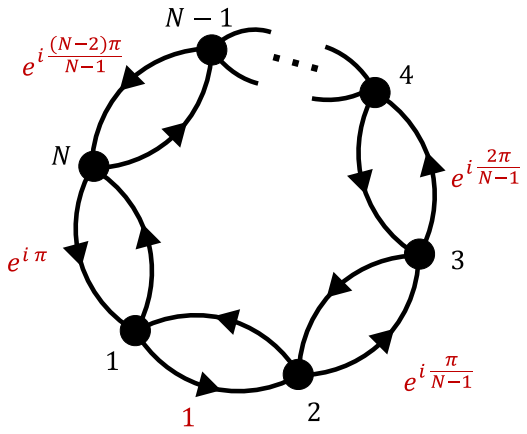

Figure 1. Proposed complex weighted cycle graph for directed transfer (complex conjugate edge weights not labelled).

To achieve directed transfer in these configurations, previous works [21, 29], stipulated that $J_{j,j+1} = J_{j+1,j} = J$, where J is some real constant for all j, while the propagation constants β_j, were also chosen such that β_j increases linearly between adjacent sites. These previous works achieved directed transfer by periodically spatially flipping the β_j, that is, $\beta_1 \leftrightarrow \beta_N, \beta_2 \leftrightarrow \beta_{N-1}, \ldots$ and so on. Hence the resulting Hamiltonian is time-dependent. We achieve essentially the same effect by making the edge weights complex and linearly increasing, while the self energy is kept constant. This keeps the Hamiltonian time independent.

In our work, we consider a graph consisting of N vertices, where the coupling is now complex $J_{j,j+1} \sim \exp(\mathrm{i}\alpha_j)$, the phase angle of the complex edge weight, α_j, increases linearly from 0 to π along consecutive edges. Unlike the cases described above, our Hamiltonian (which is based upon the adjacency matrix) is strictly time-independent.

3.1. Cycle graphs

We construct a cycle graph consisting of N vertices such that phase angle of the complex edge weights, α, increases linearly from 0 to π along consecutive edges. This is illustrated in figure 1. The adjacency matrix of the graph is given by

$$A' = \begin{bmatrix} 0 & 1 & 0 & \ldots & 0 & \mathrm{e}^{-\mathrm{i}\pi} \\ 1 & 0 & \mathrm{e}^{\mathrm{i}\frac{\pi}{N-1}} & \ldots & 0 & 0 \\ 0 & \mathrm{e}^{-\mathrm{i}\frac{\pi}{N-1}} & 0 & \ldots & 0 & 0 \\ \vdots & \ddots & \ddots & \ddots & \ddots & \vdots \\ 0 & 0 & 0 & \ldots & 0 & \mathrm{e}^{\mathrm{i}\frac{(N-2)\pi}{N-1}} \\ \mathrm{e}^{\mathrm{i}\pi} & 0 & 0 & \ldots & \mathrm{e}^{-\mathrm{i}\pi\frac{(N-2)\pi}{N-1}} & 0 \end{bmatrix}. \tag{11}$$

Instead of starting the walker at a single site we consider a normalised Gaussian wave-packet of width of $\sigma = N/10$. Evolving the Schrödiner equation (10), we plot in figure 2(a), the probability of the walker being at any given vertex as a function of time for a cycle graph with $N = 51$ vertices with weightings described as above. We observe that the wave packet move in a chiral manner—towards decreasing site numbers. One can reverse the direction of transfer by flipping the sign of all phase angles, $\mathrm{e}^{\mathrm{i}\alpha_j} \to \mathrm{e}^{-\mathrm{i}\alpha_j}$, in the Hamiltonian, as shown in figure 2(b). When the wave packet fully travels across the entire cycle no reflection occurs effectively exhibiting clockwise or counter-clockwise motion.

Recall that for bipartite graphs the introduction of directional bias is impossible if the walk is initialised at a single vertex [15, 27]. We note that cycle graphs, C_N, where N is even are bipartite and yet, directed transfer is achieved for C_N for all N using our construction and initial Gaussian packets. Furthermore we observe no key difference between the probability distributions for even and odd N unlike previous results [15, 27].

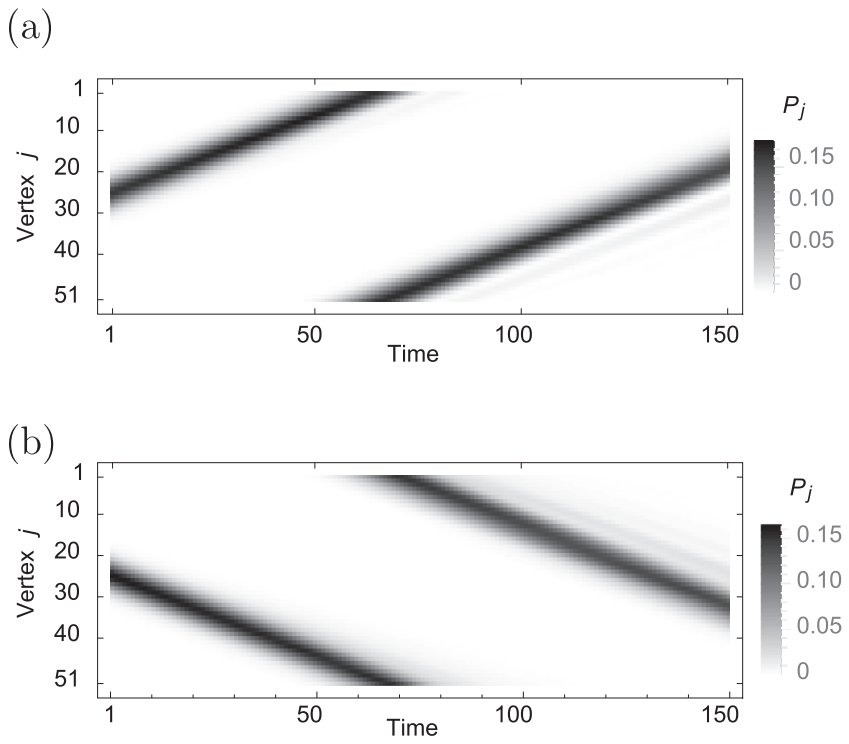

Figure 2. Probability P_j, of finding the walker at a given vertex j, as a function of time for the cycle graph with $N = 51$ vertices with ramped complex coupling weights α_j. Top plot (a) shows the probability evolving under the Hamiltonian with complex edge weights chosen as in figure 1 while bottom plot (b) shows the case where signs of all complex edge weights have been reversed.

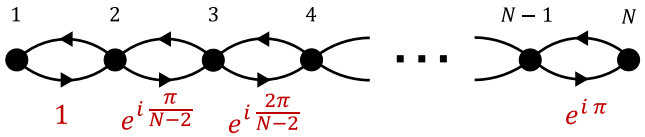

Figure 3. Complex weighted path graph that achieves directed transfer (complex conjugate edge weights not labelled).

3.2. Path graphs

One can consider 'unwrapping' the cycle graph into a path graph and adjusting edge weights such that the phase angle increases linearly from 0 to π along adjacent vertices. For path graphs, P_N, we have

$$A' = \begin{bmatrix} 0 & 1 & 0 & \dots & 0 & 0 \\ 1 & 0 & e^{i\frac{\pi}{N-2}} & \dots & 0 & 0 \\ 0 & e^{-i\frac{\pi}{N-2}} & 0 & \dots & 0 & 0 \\ \vdots & \ddots & \ddots & \ddots & \ddots & \vdots \\ 0 & 0 & 0 & \dots & 0 & e^{i\pi} \\ 0 & 0 & 0 & \dots & e^{-i\pi} & 0 \end{bmatrix}. \tag{12}$$

Figure 3 shows the path graph with N vertices with complex edge weights as given in equation (12). The phase angle increases linearly from 0 to π from left to right as depicted.

We initialise the walk on P_N, with a Gaussian wave-packet with $\sigma = \frac{N}{15}$, initially centred at $j = 25$. Figure 4 shows the probability of finding the walker at a given vertex as a function of time for P_{51}. The wave packet propagates initially towards lower indexed verticies. When the wave reaches the boundary at $j = 0$ it undergoes near perfect reflection and then propagates in the opposite direction towards larger indexed vertices. This near-perfect geometric propagation and reflection repeats every time a boundary is encountered. By reversing the sign of all complex edge weights we achieve initially directed transfer to larger indices as shown in figure 4.

Once again we note that the path graph is an example of a tree graph (and is also bipartite), and thus evolution from a single site cannot lead to directional propagation. However, our results show that

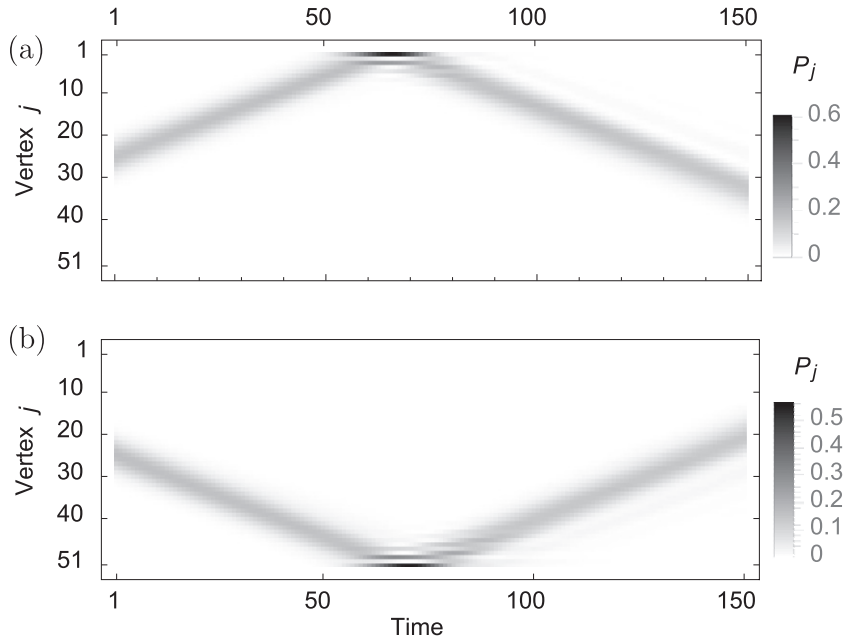

Figure 4. Directed geometric propagation and reflection of a Gaussian wave packet in a path graph. We plot the probability of measuring the walker at a given vertex as a function of time for the path graph with $N = 51$ vertices. Top plot (a) shows the results with complex edge weights as shown in figure 3 while bottom plot (b) shows the case where signs of all complex edge weights have been reversed.

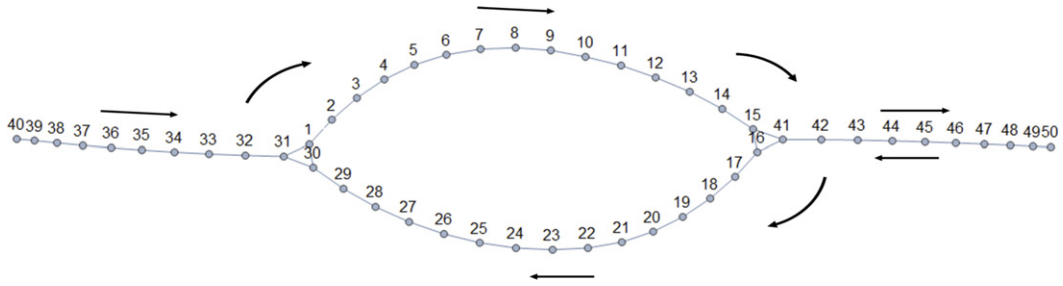

Figure 5. The circular graph, which combines path and cycle graphs to transfer information from one path to the other. The arrows show the flow of energy—excitations input onto the central cycle from the left path graph flow in a counterclockwise manner and exit towards the right on to the right path graph. Similarly excitations moving towards the left on to the central cycle from the right path graph flow counter clockwise and exit on to the left path graph. This operation is similar to an optical circulator.

directional bias is possible when we consider an initial Gaussian wave-packet and complex coupling weights.

3.3. Directional bias for a circulator graph

We now examine a combination of path and cycle graph, shown in figure 5, which we label as a CG. In photonics, a circulator is a non-reciprocal device which has three ports A, B, and C. Light entering a port, exits the next port e.g. $A \to B \to C \to A \ldots$. Such devices are used to decouple optical systems from back-reflections and back-propagating noise. In the CG we will see that wave-packets injected onto the cycle from the left path will flow to the right path along the top half of the cycle only. Wave-packets injected onto the cycle from the right path will flow to the left path along the bottom half of the cycle only. This action is very similar to that of an optical circulator. By tracking population in either the top or bottom halves of the cycle one can measure both the direction of flow and amount of population moving between the two path graphs.

In the graph depicted in figure 5, we have total 50 vertices, with a cycle graph of $n = 30$ vertices connected to two path graphs of $N = 10$ vertices each. The complex weights of the edges are chosen the same as in sections 3.1 and 3.2, except at the junction of cycle and the two paths. The wave-packet starts near the left most end of the left path in Gaussian state centred at vertex 35, as in figure 6, with width

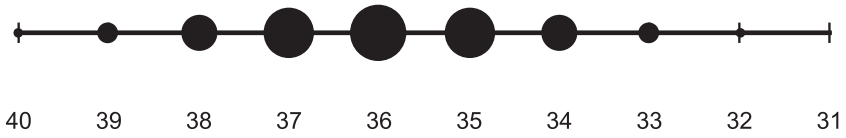

Figure 6. Example of an initial Gaussian wave packet, centred at the middle of the left path chain with site occupation indicated by the size of each disc.

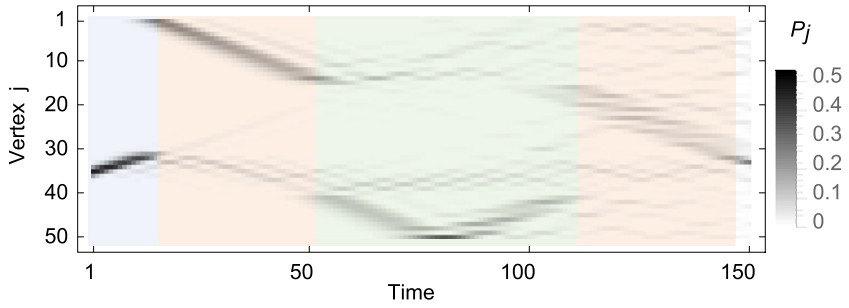

Figure 7. Probability P_j of measuring the walker at a given vertex as a function of time for the combination of cycle and path graphs with $n = 30$ vertices in cycle graphs and $N = 10$ in each of the two paths. We see that the wavepacket starts at $t = 1$ on the left path (blue), moves onto the cycle graph and circulates clockwise (orange), moves out and back on the right path graph (green), and again moves clockwise on the cycle graph (orange).

chosen as $\sqrt{2}\sigma = n/20$. The adjacency matrix of the left path portion of the graph is given by

$$\begin{aligned} A_{i,i+1} &= \mathrm{e}^{\mathrm{i}\pi(i-1)/N-2}, \\ A_{i+1,i} &= \mathrm{e}^{-\mathrm{i}\pi(i-1)/N-2}. \end{aligned} \tag{13}$$

Evolving the dynamics we find that wave-packet moves towards the junction of cycle and the left path graph. Here the weighted edges are chosen such that the junction acts as a switch. Destructive and constructive interference is engineered so that walker is aimed to move off the left path and towards the top half of the cycle graph and not towards the bottom half. This directed transfer is achieved by setting the couplings as

$$\begin{aligned} A_{30,31} &= \mathrm{e}^{-\mathrm{i}\pi/2}, \\ A_{31,30} &= \mathrm{e}^{\mathrm{i}\pi/2}, \\ A_{31,1} &= A_{1,31} = 1. \end{aligned} \tag{14}$$

This directed transfer is achieved by adjusting the phases to achieve constructive and destructive interference. As the wave-packet reaches the cycle-path junction on the right, they are directed to turn on to the right path by adjusting the couplings as

$$\begin{aligned} A_{15,16} &= \mathrm{e}^{-\mathrm{i}\pi/2}, \\ A_{16,15} &= \mathrm{e}^{\mathrm{i}\pi/2}, \\ A_{41,15} &= A_{15,41} = 1, \\ A_{41,16} &= A_{16,41} = 1. \end{aligned} \tag{15}$$

As the walk evolves we plot the probability distribution as a function of time in figure 7. We see that when the walker reaches vertex 31, they are directed towards vertex 1 and is prohibited to turn towards vertex 30. The walker then moves steadily till vertex 15 and is then directed to turn left to vertex 41 and is stopped from going to vertex 16. Once the walker hits the right end of the right path (vertex 50), they are reflected and move back towards the cycle graph moving towards the left on the right hand path. At about $t \sim 100$, they are injected onto the cycle graph through vertices 15, 16 and 41, and are 'circulated' along the bottom half of the cycle back towards the left path.

We explicitly plot the probability distribution for vertices 1, 30 and 31 in figure 8. We see that when the walker reaches the vertex 31, they are directed to vertex 1 with high probability (red curve) and the probability of transfer to vertex 30 (black curve) is very low. Similarly, we can see the comparison of

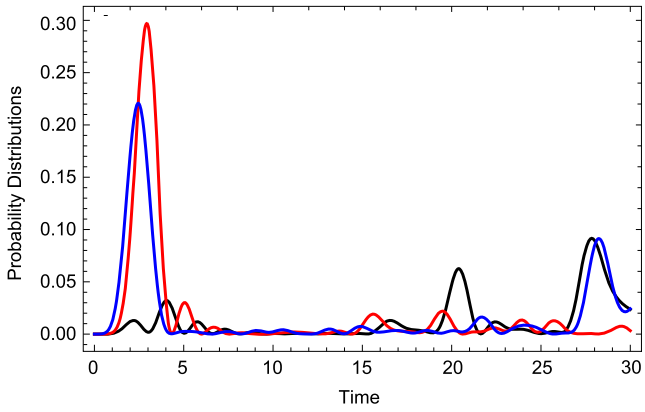

Figure 8. Switching network connecting left path graph to the cycle graph: we plot the probability of occupation as a function of time for vertices 31 (blue), 1 (red) and 30 (black). The phases of the connecting network is chosen to inject the incoming walker to flow in a clockwise fashion on the cycle.

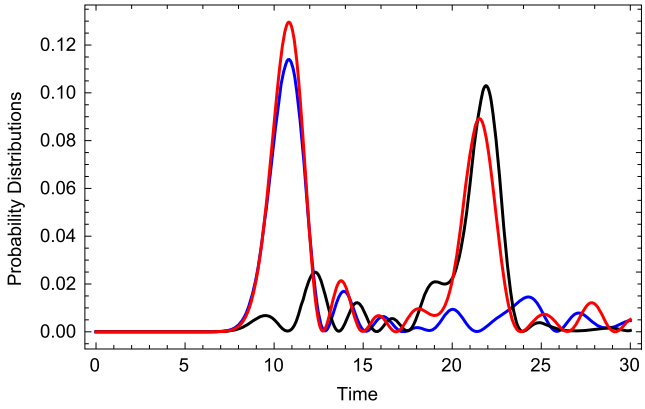

Figure 9. Switching network connecting right path graph to the cycle graph: we plot the probability of occupation as a function of time for vertices 15 (blue), 41 (red) and 16 (black). Again the phases of the connecting network is chosen to inject the incoming walker to flow in a clockwise fashion on the cycle.

probability distribution functions of vertices 15, 16 and 41 in figure 9. When the walker reaches the vertex 15, the transfer to vertex 16 is prohibited and the walker is directed to vertex 41, which appears as a peak in red curve.

4. Detection of non-Markovian process

Quantum non-Markovianity of a channel is typically identified by information back-flow. Markovian evolution involves information and energy being lost to a large environment in a manner which is never returned to the system. In a non-Markovian open system the bath possesses some finite memory time and there is some chance that information and energy will flow back into the system from the bath. We ask the question: can one detect this energy back flow from the bath back into the system? In optical systems one can use an *optical circulator*, to separate energy transport depending on the direction of transport. If one could insert a similar type of device between a system and it's environment then energy flowing into/from the bath would be separated and identified. Excitations that entered back into the system after entering the environment would indicate a non-Markovian environment. We specifically consider a zero-temperature environment which initially has no excitations but which can be tuned to be non-Markovian or Markovian. We wish to know, by looking at the energy transport and direction of energy flow between the system and the environment, if the environment is non-Markovian. We will see that by connecting the system to the environment via the above circulant graph, if the circulant graph records any energy flow along it's bottom portion, energy must be flowing back from the environment towards the system and the environment must be non-Markovian.

We can exactly simulate any type of environment via the dynamics of a semi-infinite continuous QRW [30]. To simulate a Markovian environment one considers injecting excitation at one end of this

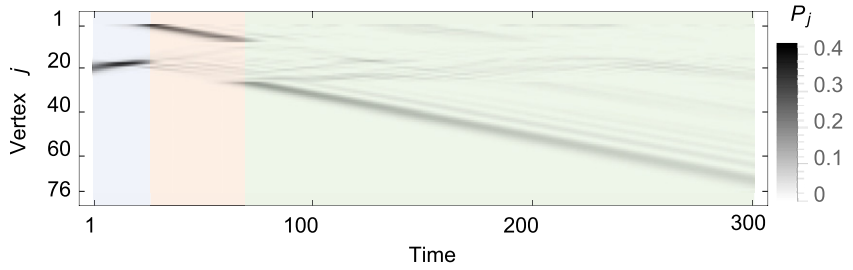

Figure 10. Model of a Markovian bath—the excitation exits the system (blue), into the cycle moving clockwise (red), and into the semi-infinite environment (green), never to return to the system. We plot the probability of the walker at a given vertex for an initial Gaussian packet with $\sigma = 16/5$ and centred at $|\psi(0)\rangle = |20\rangle$. Here $n = 16$ vertices in cycle and $N_1 = 10$ and $N_2 = 50$ in left (system) and right (environment) chain paths, respectively.

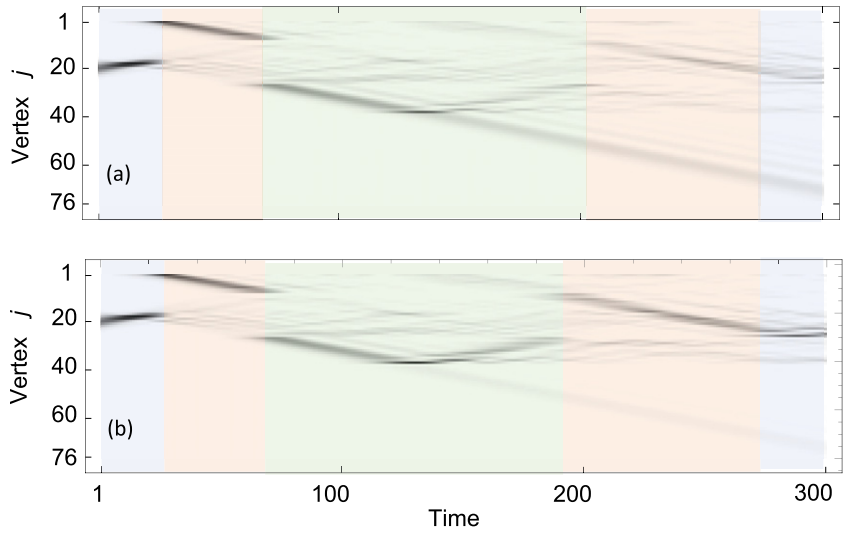

Figure 11. Modelling a non-Markovian bath: the wavepacket starts in the left (system) chain (blue), enters the CG and rotates clockwise (red), then enters the right (environment) chain (green). By altering the coupling $h_{38,39} = m$, $m \neq 1$, at the time $T \sim 130$ some of the wavepacket is reflected back into the CG where it rotates clockwise (red), and enters back into the system (blue). We choose (a) $m = 1/2$ and (b) $m = 4$. The vertex labels are the same as in figure 10.

semi-infinite chain at a rate much slower than the inter-site coupling on this semi-infinite chain. Energy injected at end-site is then transported forever away from that end-site, never to return. Such semi-infinite continuous QRWs have been used as Markovian environments to explore superradiance in harmonic oscillators [31], or to experimentally control transport in photonic networks [32].

We now make the above discussion more concrete and consider the left path chain in figure 5, to be the 'system' and the right path chain to be the 'environment', and this right path chain will be semi-infinite in length. We initialise the combined system + environment so that only the system sites are occupied. As time progresses these initial excitations will evolve and some will move through the top portion of the circulator in figure 5, and will enter the right path chain or *environment*. To simulate a Markovian environment we consider the aforementioned case where the couplings on the semi-infinite environment QRW chain are strong and all excitations injected onto this chain by the circulator move continually to the right on the semi-infinite chain to never return. In this case the lower portion of the CG in figure 5, will never be occupied.

By adjusting the specific couplings in the environment chain one can actually model any type of non-Markovian bath coupled to the system [30], and in such cases energy and information will be transferred back into the system from the environment and in doing so, they will be transported through the lower portion of the CG. Thus, any occupation in the lower half of this CG is an indication that excitations are returning from the environment and thus one can infer that the environment is non-Markovian.

For simulations we consider the CG as before, with $n = 16$ vertices in the cycle, $N_1 = 10$ in left path chain (the system chain), and $N_2 = 50$ in the right path chain (the longer environment chain). The coupling weights are adjusted as before with uniform magnitudes $h_{ij} = 1\ \forall\ i, j$ (3), and complex phases. The

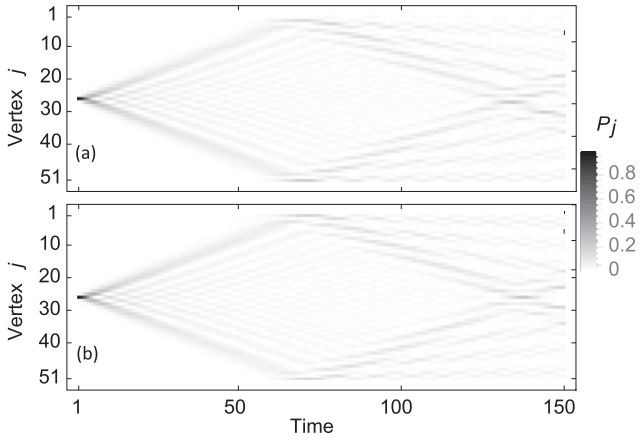

Figure 12. Momentum-position uncertainty where we choose an initial state which is highly localised in position. We plot the occupation probability as a function of time when the initial state is localised at a single vertex, $|\psi(0)\rangle = |26\rangle$. Evolution is described on a (a) the cycle graph, and (b) path graph each with $N = 51$. The momentum is totally uncertain and the walker moves with no directional bias.

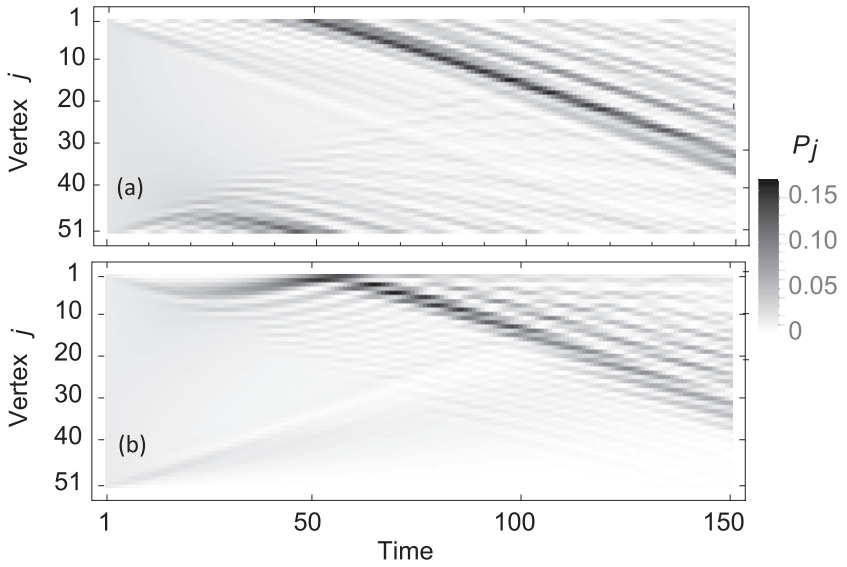

Figure 13. Momentum-position uncertainty where we choose an initial state which is highly delocalised in position. We consider identical dynamics to that shown in figure 12, but choose an initial state which is an equal superposition over all verticies for the (a) cycle and (b) path graphs. We observe that a momentum bias develops by time $T = 50$.

Gaussian wave-packet is again initialised to have support only small system chain on left. Evolving the Schrödinger equation, the wave-packet is transported along the upper half of the cycle, reaches the junction with the longer environment chain on right and flows, as before, on to the environment chain. To model a Markovian bath, where no information flows back to the system from the environment, we consider the environment right chain to be very long, essentially semi-infinite. The wave-packet never reverses direction and is never seen in the lower half of the CG, as shown in figure 10.

Information back-flow, or non-Markovian bath dynamics, can occur if the edge weights in the right (environment), path chain are altered. We change the edge weights in the middle of right chain by taking $h_{38,39} = m$, for the cases when $m = 1/2$ or $m = 4$ (the right path chain has $N_2 = 50$ vertices). We see in figure 11 that varying the weight m, at a location in the right environment path, disrupts the perfect flow of the wavepacket to the right. Instead some portion of the wavepacket is reflected back towards the CG and flows back to the left system chain along the lower half of the cycle. The non-Markovianity occurs when we alter the perfect flow along the right environment chain i.e. when $m \neq 1$.

5. Relationship with the uncertainty principle

We now uncover a deeper relation between the width of the Gaussian wave, σ, and a type of position-momentum uncertainty principle. In the case when the walk is initialised at a single vertex, analogous to a quantum particle with a certain position, we have complete uncertainty in the walker's momentum. This is illustrated in figure 12, which shows the probability of measuring the walker in time propagating on either a complex weighted cycle or complex weighted path graph. The resulting dynamics possesses a wide range of momenta, both positive and negative with no directional bias.

If the width $\sigma = O(N)$, we have an analogous situation to a particle with complete uncertainty in its position which gives completely certainty in its momentum. This is illustrated in figure 13 for the cycle and path graphs where we choose an initial state which is completely delocalised. To model a semi-localised excitation which exhibits a well defined momentum and is spatially localised we have found that numerical results suggest that $\frac{N}{20} < \sigma < \frac{N}{10}$ will suffice.

A caveat of this uncertainty principle relationship is that we can never practically achieve solitonic directional propagation. Except in the extreme case of the equal superposition state ($\sigma = O(N)$) we will always have some degree of dispersion in the travelling Gaussian wave-packet.

We thus surmise the existence of a class of initial states for our type of complex-weighted continuous QRW which appear to be similar to minimum uncertainty states in quantum optics, e.g. coherent states, whose transport has low dispersion and whose transport directionality can be well controlled.

6. Conclusions

We have proposed an experiment to achieve directed transfer in various graphs. Previously directed transfer was either achieved by considering non-unitary evolution of an open quantum system [14], or by taking a time-dependent Hamiltonian [15]. In this work we have found that through the use of an initial Gaussian state and using complex graph couplings, we can achieve directed transfer in path and cycle graphs and in a graph with a combination of the two.

We can completely suppress the transfer in a particular direction while enhancing it in a preferred direction. In a combination of path and cycle graph, which we denote as the CG, the walker is shown to occupy either the bottom or top half of the cycle depending on the direction of the packet's flow. We used this CG to demonstrate the non-Markovian nature of some type of environments—by inserting this circulator between a system and environment, the direction of flow of excitation can be monitored via the chiral-spatial nature of the CG transport. A non-Markovian environment will cause excitations to return to the system—via the lower arm of the CG. Finally we studied a type of uncertainty principle associated with using delocalised wavepackets to obtain a more certain momentum bias in the walker's transport.

Although we have studied only specific types of graphs it would be interesting to explore whether directed transport can be achieved within more general types of graphs using complex edge weights and suitable initial states. In summary, the use of wave-packets and complex weights in quantum graph-theoretic algorithms can provide a wealth of new phenomena such as biased transport and chiral propagations.

Data availability statement

All data that support the findings of this study are included within the article (and any supplementary files).

ORCID iDs

A Khalique https://orcid.org/0000-0003-4931-7415
J B Wang https://orcid.org/0000-0001-7544-0084
J Twamley https://orcid.org/0000-0002-8930-6131

References

[1] Aharonov Y, Davidovich L and Zagury N 1993 *Phys. Rev.* A **48** 1687–90
[2] Manouchehri K and Wang J B 2014 *Physical Implementation of Quantum Walks* (New York: Springer)
[3] Ren J, Chen T and Zhang X 2019 *New J. Phys.* **21** 053034
[4] Izaac J A, Wang J B and Li Z J 2013 *Phys. Rev.* A **88** 042334
[5] Izaac J A and Wang J B 2015 *Comput. Phys. Commun.* **186** 81
[6] Qiang X, Loke T, Montanaro A, Aungskunsiri K, Zhou X, O'Brien J L, Wang J B and Matthews J C F 2016 *Nat. Commun.* **7** 11511

[7] Loke T and Wang J B 2017 *J. Phys. A: Math. Theor.* **50** 5
[8] Farhi E and Gutmann S 1998 *Phys. Rev.* A **58** 915–28
[9] Childs A M 2009 *Phys. Rev. Lett.* **102** 180501
[10] Sánchez-Burillo E, Duch J, Gómez-Gardeñes J and Zueco D 2012 *Sci. Rep.* **2** 605
[11] Whitfield J D, Rodríguez-Rosario C A and Aspuru-Guzik A 2010 *Phys. Rev.* A **81** 022323
[12] Falloon P E, Rodriguez J and Wang J B 2017 *Comput. Phys. Commun.* **217** 162
[13] Matwiejew E and Wang J 2021 *Comput. Phys. Commun.* **260** 107724
[14] Lindblad G 1976 *Commun. Math. Phys.* **48** 119–30
[15] Zimborás Z, Faccin M, Kádár Z, Whitfield J D, Lanyon B P and Biamonte J 2013 *Sci. Rep.* **3** 2361
[16] Izaac J A, Wang J B, Abbott P C and Ma X S 2017 *Phys. Rev.* A **96** 032305
[17] Wu T, Izaac J A, Li Z-X, Wang K, Chen Z-Z, Zhu S, Wang J B and Ma X-S 2020 *Phys. Rev. Lett.* **125** 240501
[18] Chen T, Wang B and Zhang X 2017 *New J. Phys.* **19** 113049
[19] Wang K, Shi Y, Xiao L, Wang J, Joglekar Y N and Xue P 2020 *Optica* **7** 1524
[20] Sett A, Pan H, Falloon P E and Wang J B 2019 *Quantum Inf. Process.* **18** 159
[21] Javaherian C and Twamley J 2017 *Opt. Express* **25** 25970–9
[22] Manouchehri K and Wang J B 2007 *J. Phys. A: Math. Theor.* **40** 13773
[23] Wang J B and Scholz T T 1998 *Phys. Rev.* A **57** 3554
[24] von Luxburg U 2007 *Stat. Comput.* **17** 395–416
[25] Godsil C and Royle G F 2001 *Algebraic Graph Theory* (Berlin: Springer)
[26] Ambainis A 2003 *Int. J. Quantum Inform.* **01** 507–18
[27] Lu D *et al* 2016 *Phys. Rev.* A **93** 042302
[28] Mülken O and Blumen A 2011 *Phys. Rep.* **502** 37–87
[29] Morandotti R, Peschel U, Aitchison J S, Eisenberg H S and Silberberg Y 1999 *Phys. Rev. Lett.* **83** 4756–9
[30] Woods M P, Groux R, Chin A W, Huelga S F and Plenio M B 2014 *J. Math. Phys.* **55** 032101
[31] Delanty M, Rebić S and Twamley J 2012 *Eur. Phys. J.* D **66** 93
[32] Biggerstaff D N *et al* 2016 *Nat. Commun.* **7** 11282